Generation of a periodic array of radially polarized plasmonic focal spots

Jonathan Bar-David, Gilad M. Lerman, Liron Stern, Noa Mazurski, and Uriel Levy*

Department of Applied Physics, The Benin School of Engineering and Computer Science, The Hebrew University of Jerusalem, Jerusalem, 91904, Israel

ulevy@cc.huji.ac.il

Abstract: This paper demonstrates experimentally the tight focusing of a 3X3 array of radially polarized diffraction orders, and the coupling of this array of spots to surface plasmon polaritons (SPPs), propagating on a uniform metal film, and effectively generating a periodic structure of plasmonic sources by the use of structured illumination pattern, rather than by structuring the plasmonic sample. Using near field measurements, we observed coherent interactions between these multiple plasmonic sources as they propagate towards each other. The demonstrated setup exploits the previously demonstrated advantages of radially polarized light in coupling to SPPs and in generating sharper plasmonic hot spots and expends its use towards mitigating parallel processing challenges. The experimental results are in good agreement with the theory, showing interference fringes having periodicity compatible with the plasmonic SPP wavelength. The demonstrated approach of generating array of hot spots on flat metallic films is expected to play a role in variety of applications, e.g. microscopy, lithography, sensing and optical memories.

OCIS codes: (050.1950) Diffraction gratings; (240.6680) Surface plasmons; (260.3160) Interference.

References and links

1. "Editorial, "Surface plasmon resurrection," Nat. Photonics **6**, 707 (2012).
2. M. L. Brongersma and V. M. Shalaev, "Applied physics. The case for plasmonics," Science **328**(5977), 440–441 (2010).
3. E. Ozbay, "Plasmonics: Merging photonics and electronics at nanoscale dimensions," Science **311**(5758), 189–193 (2006).
4. M. I. Stockman, "Nanoplasmonics: past, present, and glimpse into future," Opt. Express **19**(22), 22029–22106 (2011).
5. D. K. Gramotnev and S. I. Bozhevolnyi, "Plasmonics beyond the diffraction limit," Nat. Photonics **4**(2), 83–91 (2010).
6. S. Kawata, Y. Inouye, and P. Verma, "Plasmonics for near-field nano-imaging and superlensing," Nat. Photonics **3**(7), 388–394 (2009).
7. R. W. Boyd and D. J. Gauthier, "Controlling the velocity of light pulses," Science **326**(5956), 1074–1077 (2009).
8. J. A. Schuller, E. S. Barnard, W. Cai, Y. C. Jun, J. S. White, and M. L. Brongersma, "Plasmonics for extreme light concentration and manipulation," Nat. Mater. **9**(3), 193–204 (2010).
9. M. Kauranen and A. V. Zayats, "Nonlinear plasmonics," Nat. Photonics **6**(11), 737–748 (2012).
10. Z. Liu, J. M. Steele, W. Srituravanich, Y. Pikus, C. Sun, and X. Zhang, "Focusing Surface Plasmons with a Plasmonic Lens," Nano Lett. **5**(9), 1726–1729 (2005).
11. A. Yanai and U. Levy, "Plasmonic focusing with a coaxial structure illuminated by radially polarized light," Opt. Express **17**(2), 924–932 (2009).
12. G. M. Lerman, A. Yanai, and U. Levy, "Demonstration of Nanofocusing by the use of Plasmonic Lens Illuminated with Radially Polarized Light," Nano Lett. **9**(5), 2139–2143 (2009).
13. W. Chen and Q. Zhan, "Realization of an evanescent Bessel beam via surface plasmon interference excited by a radially polarized beam," Opt. Lett. **34**(6), 722–724 (2009).
14. P. Ginzburg, A. Nevet, N. Berkovitch, A. Normatov, G. M. Lerman, A. Yanai, U. Levy, and M. Orenstein, "Plasmonic Resonance Effects for Tandem Receiving-Transmitting Nanoantennas," Nano Lett. **11**(1), 220–224 (2011).

#181718 - $15.00 USD Received 13 Dec 2012; revised 17 Jan 2013; accepted 21 Jan 2013; published 6 Feb 2013

15. A. Normatov, P. Ginzburg, N. Berkovitch, G. M. Lerman, A. Yanai, U. Levy, and M. Orenstein, "Efficient coupling and field enhancement for the nano-scale: plasmonic needle," Opt. Express **18**(13), 14079–14086 (2010).
16. B. Desiatov, I. Goykhman, and U. Levy, "Nanoscale Mode Selector in Silicon Waveguide for on Chip Nanofocusing Applications," Nano Lett. **9**(10), 3381–3386 (2009).
17. M. I. Stockman, "Nanofocusing of optical energy in tapered plasmonic waveguides," Phys. Rev. Lett. **93**(13), 137404 (2004).
18. E. Verhagen, L. Kuipers, and A. Polman, "Enhanced nonlinear optical effects with a tapered plasmonic waveguide," Nano Lett. **7**(2), 334–337 (2007).
19. F. De Angelis, G. Das, P. Candeloro, M. Patrini, M. Galli, A. Bek, M. Lazzarino, I. Maksymov, C. Liberale, L. C. Andreani, and E. Di Fabrizio, "Nanoscale chemical mapping using three-dimensional adiabatic compression of surface plasmon polaritons," Nat. Nanotechnol. **5**(1), 67–72 (2010).
20. C. Ropers, C. C. Neacsu, T. Elsaesser, M. Albrecht, M. B. Raschke, and C. Lienau, "Grating-coupling of surface plasmons onto metallic tips: a nanoconfined light source," Nano Lett. **7**(9), 2784–2788 (2007).
21. A. Bouhelier, F. Ignatovich, A. Bruyant, C. Huang, G. Colas des Francs, J.-C. Weeber, A. Dereux, G. P. Wiederrecht, and L. Novotny, "Surface plasmon interference excited by tightly focused laser beams," Opt. Lett. **32**(17), 2535–2537 (2007).
22. W. Chen, D. C. Abeysinghe, R. L. Nelson, and Q. Zhan, "Plasmonic Lens Made of Multiple Concentric Metallic Rings under Radially Polarized Illumination," Nano Lett. **9**(12), 4320–4325 (2009).
23. Q. Zhan, "Cylindrical vector beams: from mathematical concepts to applications," Adv. Opt. Photon. **1**(1), 1–57 (2009).
24. Q. Zhan, "Evanescent Bessel beam generation via surface plasmon resonance excitation by a radially polarized beam," Opt. Lett. **31**(11), 1726–1728 (2006).
25. A. Yanai and U. Levy, "The role of short and long range surface plasmons for plasmonic focusing applications," Opt. Express **17**(16), 14270–14280 (2009).
26. L. Novotny and B. Hecht, "Principals of Nano-Optics," Cambridge University Press, Cambridge, 2007.
27. M. Born and E. Wolf, "Fundamentals of optics," (Pergamon, 1959).
28. J. W. Goodman, "Introduction to Fourier Optics," (McGraw-Hill, 1996).
29. H. Dammann and K. Gortler, "High-efficiency in-line multiple imaging by means of multiple phase holograms," Opt. Commun. **3**(5), 312–315 (1971).
30. C. Zhou and L. Liu, "Numerical study of Dammann array illuminators," Appl. Opt. **34**(26), 5961–5969 (1995).
31. L. Aigouy, P. Lalanne, J. P. Hugonin, G. Julié, V. Mathet, and M. Mortier, "Near-Field Analysis of Surface Waves Launched at Nanoslit Apertures," Phys. Rev. Lett. **98**(15), 153902 (2007).
32. H. F. Schouten, N. Kuzmin, G. Dubois, T. D. Visser, G. Gbur, P. F. A. Alkemade, H. Blok, G. W. Hooft, D. Lenstra, and E. R. Eliel, "Plasmon-Assisted Two-Slit Transmission: Young's Experiment Revisited," Phys. Rev. Lett. **94**(5), 053901 (2005).

1. Introduction

In the last two decades the field of plasmonics is flourishing as evident by the rapid growth in number of publications [1]. Many of the latest achievements are discussed in several excellent review papers [2–9]. Typically, plasmonic devices are designed to operate under linearly polarized light excitation. However, it was already demonstrated that in some cases, radially polarized light is the preferred choice of excitation. For example, it was shown that radially polarized light excitation (or its 1-D equivalent, namely the anti symmetric waveguide mode) plays a beneficial role in plasmonic lenses, metallic nanotapers and plasmonic excitation at a flat metallic surface by tight focusing of light through an oil immersion lens, as compared with linearly polarized light excitation [10–23].

In this work we exploit the previously demonstrated advantages of radially polarized light in coupling to SPPs and in generating sharper plasmonic hot spots and expend its use towards mitigating parallel processing challenges by generating a periodic array of coherent, radially polarized "plasmonic focal spots". This is achieved by passing a single radially polarized beam through a Dammann grating, effectively splitting the beam to multiple, equal-intensity radially polarized diffraction orders. These diffraction orders are then tightly focused on a uniform metal film, facilitating their coupling into SPPs. Using a near field scanning optical microscope (NSOM) we observed the propagation of SPP modes originated by the radially polarized diffraction orders and the coherent interactions between these "plasmonic sources" as they propagate on the metal film.

This paper is structured as follows: section 2 describes the theoretical background of light confinement and its conversion into plasmonic focal spots, section 3 presents the computer

#181718 - $15.00 USD Received 13 Dec 2012; revised 17 Jan 2013; accepted 21 Jan 2013; published 6 Feb 2013

simulations showing the expected intensity interference pattern on the metal film. In section 4 we describe our experimental setup, and section 5 presents the experimental results. In section 6 we discuss the suppression of coherent interactions by increasing the propagation loss of the plasmonic mode. Section 7 concludes the paper.

2. Theoretical background

When light is tightly focused through glass onto a thin metal film which is evaporated on the glass, and phase-matching conditions are met, it can be coupled to SPP's propagating on the other interface of the metal, i.e. the interface between metal and air.

This coupling scheme is now well established, both theoretically and experimentally [13, 21, 24, 25]. While in principle the tight focused field should be calculated by integrating over all diffraction angles ranging from zero to the numerical aperture of the microscope objective, in practice only very small range of angles which satisfy the phase matching conditions will contribute to the coupling of tight focused light into SPPs. Under such circumstances, it has been shown that when the incident light is radially polarized, the SPP near-field will take the form of Bessel functions [21, 24, 25], with a "plasmonic focal-spot" on the optical axis, with high confinement of optical field and energy:

$$E_{\hat{z}}(r, z=0) \propto AJ_0(\beta r) \tag{1}$$

$$E_{\hat{r}}(r, z=0) \propto -iA\frac{k_D}{\beta}J_1(\beta r) \tag{2}$$

Here $\hat{Z}$ is the out-of-plane field component (z = 0 is the metal-air interface), and $\hat{r}$ is the in-plane component, β is the SPP propagation coefficient and k_D is the SPP decay coefficient in the $\hat{Z}$ direction. In the experimental setup we shall later describe, for illumination at wavelength λ = 975 nm, we have calculated $|\beta| = 6.49\ \mu m^{-1}$; $|k_D| = 0.77\ \mu m^{-1}$, meaning that $E_{\hat{z}}$ is the dominant field component, and it is ~10 times stronger than $E_{\hat{r}}$.

However, when measuring these fields with an aperture type NSOM, the $E_{\hat{z}}$ component is only weakly coupled [2, 5, 7] to the tip and therefore the measurement typically consists of a combination of both field components, with ratio that is depending on the specific NSOM probe. In some cases, the dominant field component will be, surprisingly, the in-plane field component - $E_{\hat{r}}$. In the following we will be consistent with previous papers [13, 21, 26], assuming that the transverse field component (which is proportional to the transverse derivative of the z polarized field component) is dominant in the NSOM image.

When tightly focusing multiple beams diffracted from a diffraction grating, each beam propagates with a slightly different angle (measured from the optical axis and defined by the ratio of wavelength to the period of the grating), and should be focused to a different point in the focal plane (see Fig. 1) [27, 28]. If each of these beams is radially polarized, we expect to obtain multiple plasmonic sources propagating along the metal-air interface, each with a cylindrical symmetry with respect to the origin of the plasmonic spot. Furthermore, due to the coherence between these sources, they are expected to interfere, generating an interference pattern which depends on their distances, the plasmonic wavelength and the initial phase of each plasmonic source. This effect is observed and discussed in the following sections.

3. Simulation

To calculate the obtained plasmonic field propagating along the metal-air interface we assumed 9 plasmonic sources, set in a 3X3 array with a spacing of 8 μm. Each source generates a field pattern given by Eq. (2). To better fit the simulation to the actual experimental scenario (described in more details in the next two sections), we assumed that

#181718 - $15.00 USD Received 13 Dec 2012; revised 17 Jan 2013; accepted 21 Jan 2013; published 6 Feb 2013

the amplitude of the central spot is larger by a factor of $\sqrt{2}$ from the amplitudes of the other spots. The phase of each plasmonic source is resulted from the properties of the grating generating the diffraction orders. The phase of each diffraction order was numerically calculated from the Fourier transform of the grating structure. For our structure, the phase difference between the (nth, mth) diffraction order and the 0th order is:

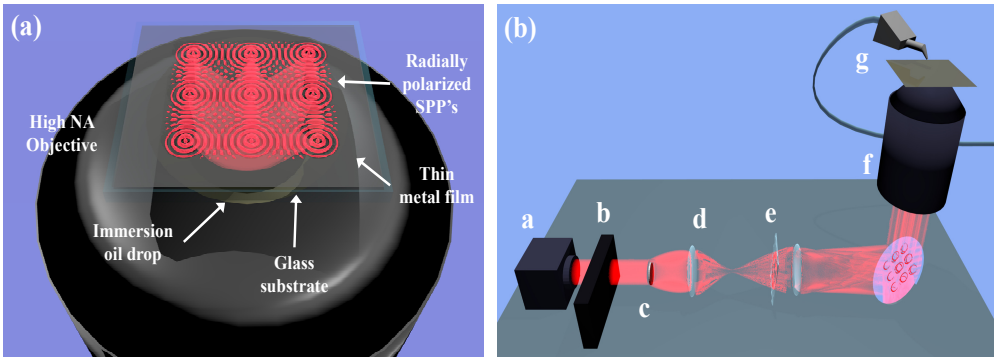

Fig. 1. (a) Illustration of SPP coupling scheme: Radially polarized laser beams are focused by a high NA oil-immersion microscope objective onto a microscope cover slip coated with a 50 nm thick Gold (Au) film. SPP's are coupled to the Gold-Air interface. (b) Experimental setup: A laser beam (a) propagates through a radial polarization converter (b). The center of the beam is blocked by metallic disk (c), the beam is expanded by an inverted telescope (d) and diffracted by a Dammann phase grating (e). The diffraction orders propagate towards a 100X, NA = 1.4 microscope objective (f), focused on to the thin metal film, and measured by an aperture NSOM (g).

$$\phi_{n,m} = 2.278(n+m) \; for \; n,m = 0,\pm 1 \qquad (3)$$

The obtained plasmonic field pattern, calculated for the vacuum wavelength of 975 nm, is given by the vector sum of the contributions from all 9 plasmonic sources. The intensity of the calculated field is presented in Fig. 2. For the calculation we assumed attenuation coefficient of $\frac{1}{20}\mu m^{-1}$. While this loss coefficient is higher than the predicted Ohmic loss for a single gold-air interface, we believe it better reflects a real life scenario, in which additional losses due to scattering and metal imperfections are evident.

As can be observed from the distinct interference patterns, the plasmonic sources are interacting coherently with each other. The strength of these interactions depends on the distance between the spots, with respect to the attenuation length. This will be discussed in section 6. Additionally, we note that the pattern is not symmetric under rotation by 90 degrees. This is because of the phase difference between the various diffraction orders.

4. Experimental setup

To experimentally observe the effect of coherent interactions and to demonstrate the generation of multiple radially polarized plasmonic sources, we constructed the experimental setup depicted in Fig. 1(b). A collimated, linearly polarized beam derived from a diode laser source at the wavelength of 975 nm (Optoenergy Inc.), propagates through a radially polarized converter (Arcoptix S.A.).

Behind the polarization converter the center of the beam is blocked by a glass plate with a metallic disk on it. The position of the mask along the light propagation axis is chosen to satisfy imaging condition between the mask and the back aperture of the microscope objective, and the disk size is chosen such that it will block most of the back aperture of the objective. Next, the beam is expanded by an inverted telescope which is designed such that its front focal plane coincides with the back aperture of a microscope objective. A Dammann

#181718 - $15.00 USD Received 13 Dec 2012; revised 17 Jan 2013; accepted 21 Jan 2013; published 6 Feb 2013

phase grating is situated between the telescope's lenses splitting the beam into multiple diffraction orders.

A 100X oil-immersion objective with NA = 1.4 (Nikon PLAN APO), is used to focus these diffraction orders on the microscope cover slip sample (glass, #0, thickness ~0.1 mm, coated with 50 nm thick uniform layer of Au).

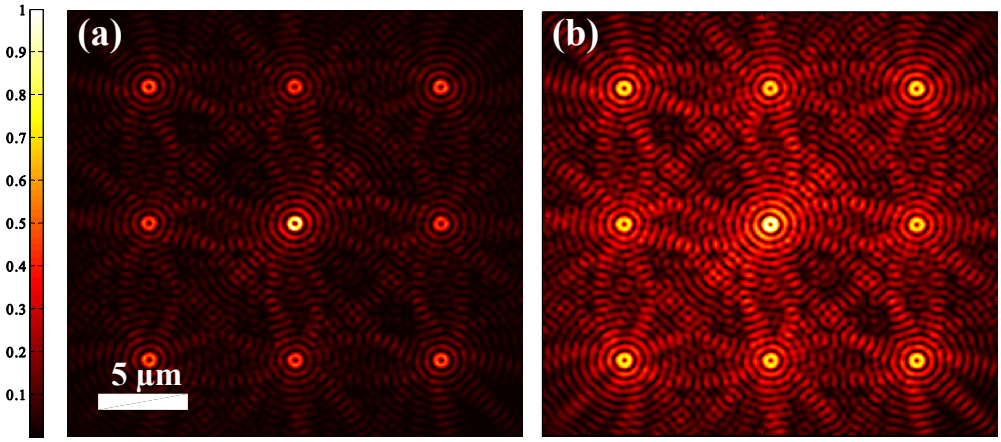

Fig. 2. Calculated intensity of the transverse plasmonic electric field showing the interaction of 9 radially polarized plasmonic sources propagating on a gold-air interface. a) Normal intensity color scale. b) Logarithmic color scale for better visibility of details.

Due to the tight focusing scheme, phase-matching condition for the SPP mode propagating on the Au-air interface is achieved and thus the illuminating beam of light is coupled to this SPP mode. The near-field of the SPPs is collected by an NSOM, (Nanonics Imaging Ltd. Multiview 4000), using Cr-Au coated NSOM probes, with typical aperture diameters of 250-300 nm. The collected signal is detected and amplified by an IR femto-Watt InGaAs photoreceiver (New-focus Inc. model 2153) connected to a lock-in amplifier (Stanford Research Systems Inc. SR830). To operate the lock-in scheme the laser beam is externally modulated at 580 Hz.

5. Experimental results

Dammann gratings are well known for their capability of splitting an optical beam into multiple diffraction orders with equal intensity [29, 30]. We have designed the gratings to produce 9 equal-intensity diffraction orders in a 3X3 array. We designed two grating structures with period lengths of $\Lambda_1 = 100\mu m$ and $\Lambda_2 = 400\mu m$ Ultimately only the latter was used, due to the shorter lateral distances between diffraction orders. Optimal phase-transition point was calculated to be $ax_1 = 0.735\Lambda$, and the grating height was designed to provide π phase delay. This calculation was confirmed by comparing with [30].

The gratings were fabricated by photolithography followed by reactive ion etching to transfer the pattern into glass. First, a 100 nm thick layer of Chromium (Cr) was deposited on the glass substrate. Next, a photo resist (S1800 series) was spun on top of the metal layer and exposed to a photomask. The pattern was transferred to the Cr layer by Cr etching which in turn was used as a mask for the reactive ion etching of the glass. Grating depth in the glass was ~1.2µm which translates to the desired phase-shift of nearly.π

The gratings were characterized by placing them in the back focal plane of a lens with focal length f = 10 cm, and placing a CCD camera in the front focal plane. Illuminating from behind the grating generates the exact Fourier transform of the grating on the CCD (see Fig.

#181718 - $15.00 USD Received 13 Dec 2012; revised 17 Jan 2013; accepted 21 Jan 2013; published 6 Feb 2013

3). Figure 3(a) shows the array of donut shaped radially polarized diffraction orders. Figure 3(b) shows the same image, now with a linear polarizer placed in front of the CCD.

As can be seen, two lobes appear along the axis for which the direction of the radial polarization coincides with the polarizer axis. Rotating the analyzer by 90 degrees results in similar rotation of the two lobes. Measuring the intensity of each diffraction order we found that the central (0th) order is 15% brighter than other orders, due to imperfections in the fabrication.

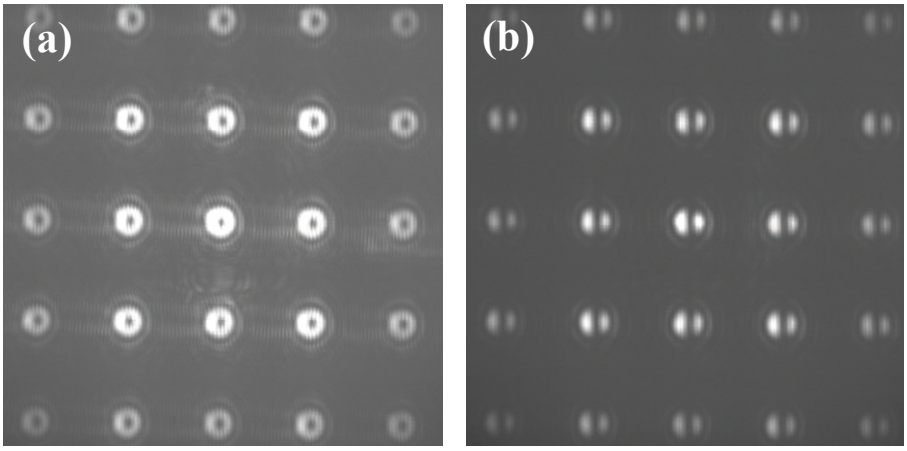

Fig. 3. (a) Far-field diffraction image of a radially polarized beam after passing through the Dammann grating. (b) Same as (a) but with a linear polarizer (aligned to block the vertical polarization component) placed in-front of the CCD.

After verifying the operation of the Dammann grating, we turned into the near field measurements of the SPPs on the metal film. First, we illuminated the sample with a single radially polarized beam, following the concept presented in [13]. The results are presented in Fig. 4. Figure 4(a) shows the NSOM scan over an area of 10 by 10 microns. Figure 4(b) shows a cross section along the white dashed line of Fig. 4(a). The experimental result agrees quantitatively (in period) and qualitatively (in intensity) with the theoretical fit derived from Eq. (2).

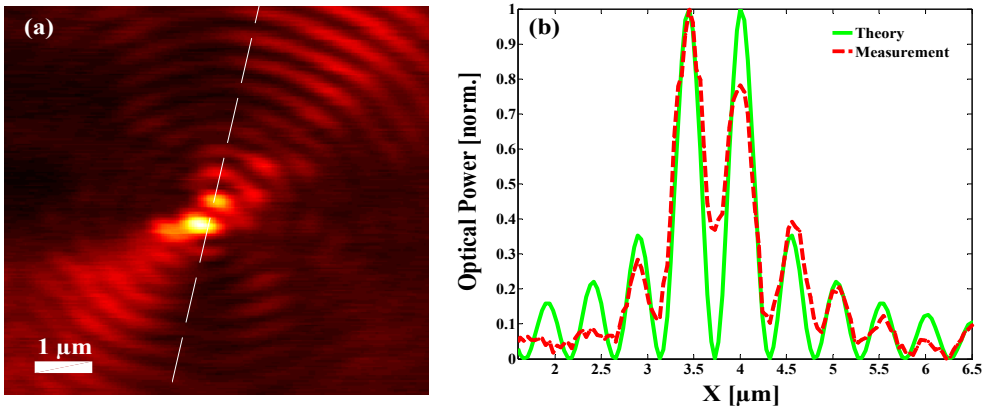

Fig. 4. (a) An NSOM scan of a single plasmonic focal spot. (b) Dashed red line - a cross section of the measured result presented in Fig. 4(a) along the white dashed line. Solid green line – the theoretical intensity pattern expected from Eq. (2).

Next, we repeated the measurement, this time with the Dammann grating presented in the optical path to obtain the 3X3 spot array. The NSOM measurement results are displayed in

#181718 - $15.00 USD Received 13 Dec 2012; revised 17 Jan 2013; accepted 21 Jan 2013; published 6 Feb 2013

linear scale (Fig. 5(a)) and in logarithmic scale (Fig. 5(b)). One can clearly observe the interference patterns between the different diffraction orders, which are the result of the coherent interactions between the multiple radially polarized plasmonic sources. While coherent interactions on flat metallic surfaces were demonstrated before, e.g. using excitation from multiple nanoslits [31, 32], this is the first time that the multiple plasmonic sources are generated by the structured illumination function rather than by patterning the sample. By comparing the experimental results to the computer simulation (Fig. 2), common features can be clearly identified in spite of the fact that the higher diffraction orders are less noticeable than expected. Possible explanations are discussed in the next paragraph. Additionally, the experimental results show strong response for light polarized along the diagonal axis running from the lower left to the upper right corner of the figure. We attribute this observation to the effect of polarization response in our NSOM probes. These probes are bended, with their bending axis perpendicular to the above mentioned diagonal. As a result, the signal polarized along the bending axis is suppressed upon propagation in the bended probe. To account for this effect we re-sketch Fig. 2, this time after taking into account the effect of polarization selective collection efficiency. The results are shown in Fig. 5(c) (in linear scale) and Fig. 5(d) (in logarithmic scale). The nice agreement between experiment and theory can now be clearly observed.

To further stress the agreement between experiment and theory, we plot a cross section of the experimental result along the white dashed line shown in Fig. 5(a), together with the theoretical cross section taken from Fig. 5(c). The results are presented in Fig. 6.

Comparing the two curves, one can see that both the interference fringes and the general trend of the envelope function are in good agreement.

As previously mentioned, an interesting observation is that the central spot appears to be almost three times stronger with respect to the other spots. The difference cannot be explained by the deviations of diffraction efficiencies in our Dammann grating (15%). Clearly, the coherent interactions between the different diffraction orders via SPP modes generate differences between the intensities of the focal spots. However, if we allocate similar amplitude to all diffraction orders we still do not observe such a drastic intensity difference in the simulation. In order to observe this difference in intensity we allocated a $\sqrt{2}$ larger amplitude value to the central diffraction order, as previously mentioned in the simulation section. We believe that the need to allocate different values of amplitude to different plasmonic spots may be the result of a difference in coupling efficiency of the various diffraction orders to SPPs. This may be attributed to the effect of coherent interaction on the coupling efficiency, as previously reported in [30, 31]. While the coupling efficiency of a single diffraction order into an SPP mode is estimated to be in the order of 1%, this efficiency can be varied by the presence of other diffraction orders via the mechanism of coherently controlled coupling. Future research should be devoted to study this issue in more details.

#181718 - $15.00 USD Received 13 Dec 2012; revised 17 Jan 2013; accepted 21 Jan 2013; published 6 Feb 2013

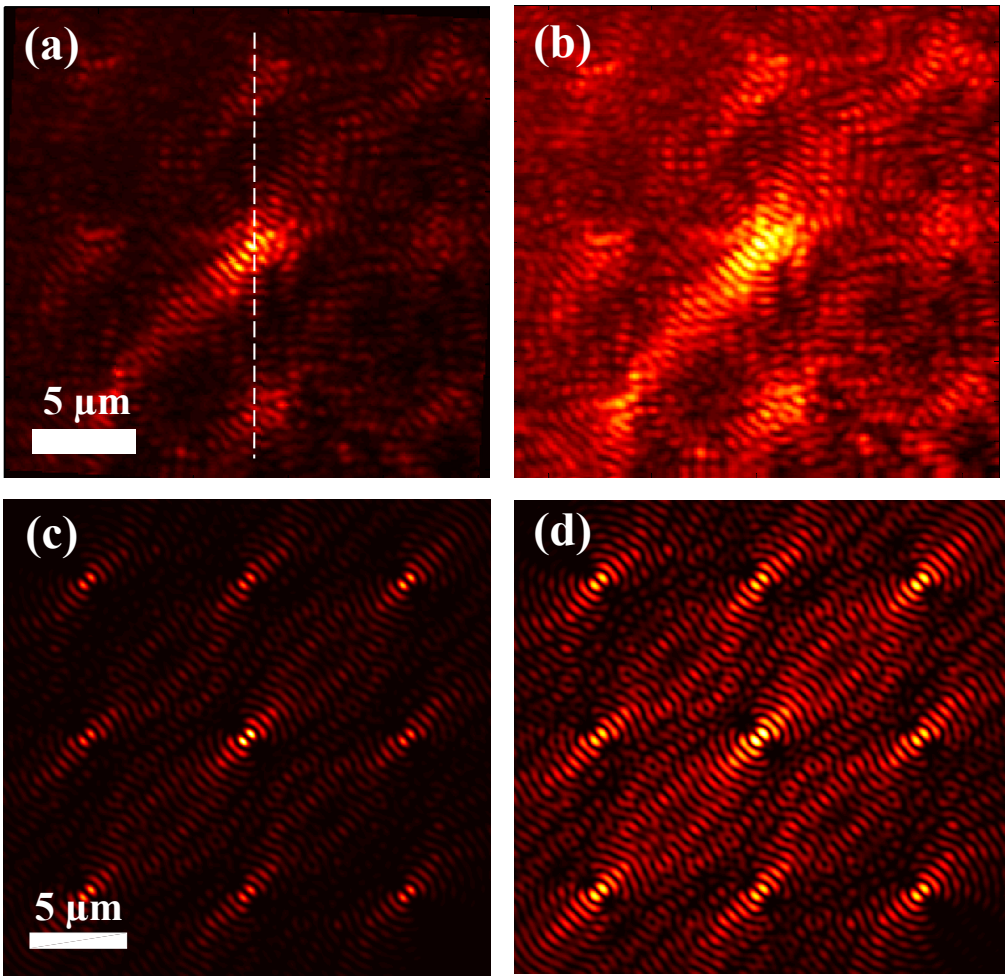

Fig. 5. (a) NSOM scan of the metal film illuminated by a 3X3 spot array in normal intensity scale. The dashed line provides a mark for the cross section presented in the next Figure. (b) Same as (a) but in logarithmic scale for better visibility of the interference fringes. (c) Simulation results showing the calculated intensity of the transverse electric field component. A polarizer was applied to transmit only the polarization direction aligned with the diagonal from lower left to the upper right of the Figure, taking into account the polarization properties of our bended NSOM probes. (d) Same as (c) but in logarithmic scale for better visibility of the interference fringes.

#181718 - $15.00 USD Received 13 Dec 2012; revised 17 Jan 2013; accepted 21 Jan 2013; published 6 Feb 2013

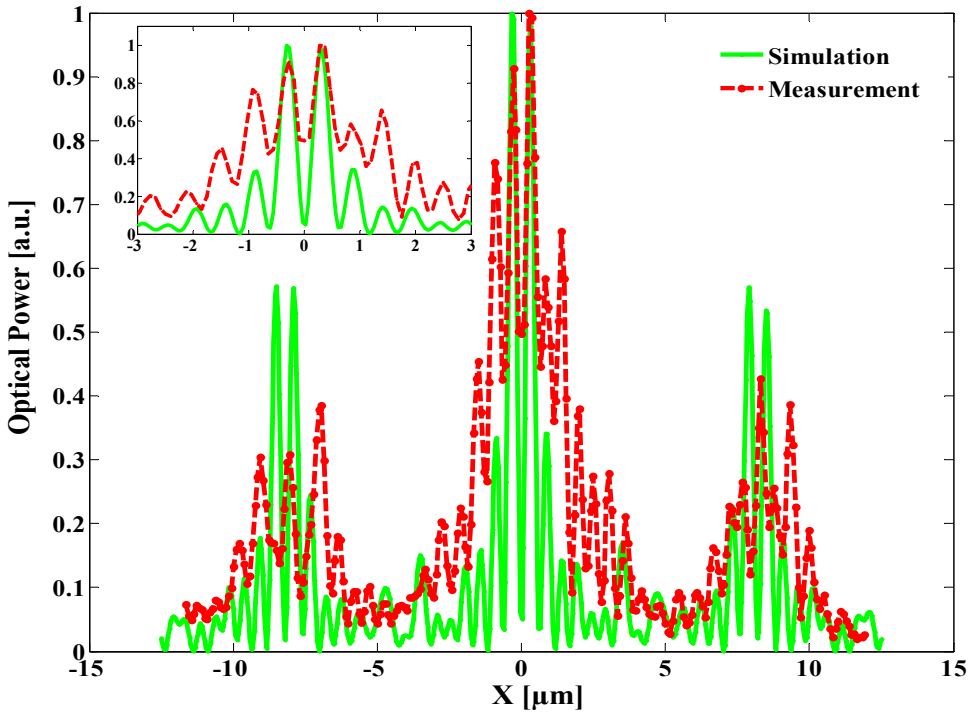

Fig. 6. Cross-sections extracted from the NSOM scan of Fig. 5(a) (dashed red line) and from the simulation results of Fig. 5(c) (solid green line) along the white dashed line marked in Fig. 5(a). Inset – Zoom in on the central region.

6. Effect of loss on the strength of the coherent interactions

The coherent in-plane interactions between SPP's originated from the array of plasmonic focal spots is an interesting result of our experimental setup. The nature of these interactions is closely related to the properties of the metal. Specifically, the ratio of the distance between the various plasmonic sources with respect to the attenuation length of the SPP mode propagating on the surface is a crucial parameter. If this ratio is small, loss is not expected to play a significant role and the interference pattern would show high visibility. With the increase of loss (or equivalently increasing the distance between the diffraction orders), the visibility of the interference fringes is expected to be suppressed.

To demonstrate how the plasmonic diffraction pattern varies as a function of the propagation loss, we plot in Fig. 7 the calculated diffraction pattern for various values of propagation loss, ranging from the case of a lossless metal to a very high loss metal (propagation length of 1 micron). As expected, the interference patterns are suppressed when the loss is increased and can barely be observed for propagation length shorter than 5 microns. Comparing Fig. 7 to our experimental results, we find that the scenario of loss coefficient of $0.05\mu m^{-1}$ seems to provide the best fit.

#181718 - $15.00 USD Received 13 Dec 2012; revised 17 Jan 2013; accepted 21 Jan 2013; published 6 Feb 2013

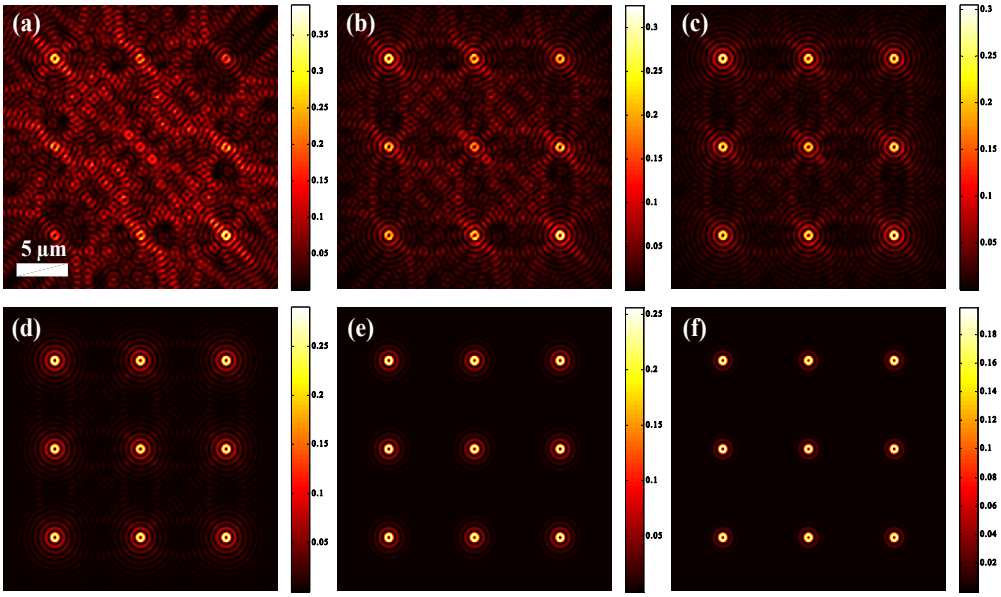

Fig. 7. Calculated intensity of the transverse plasmonic electric field showing the interaction of 9 radially polarized plasmonic sources propagating on a gold-air interface In each of the panels (a-f) a different loss coefficient was used: 0, 0.05, 0.1, 0.2, 0.5, 1 μm^{-1} . The interactions between plasmonic focal spots are suppressed with the increase in loss coefficient. Here we assumed equal amplitude for all 9 plasmonic sources.

7. Conclusions

We have demonstrated the coupling of an array of radially polarized beams to surface plasmon polaritons (SPPs) propagating on a uniform Au film. This was achieved by splitting a radially polarized beam using a phase Dammann grating into 3X3 array of diffraction orders which are tightly focused onto the metal film with the aid of a high N.A oil immersion microscope objective.

The demonstrated setup allows taking advantage of the previously demonstrated advantages of radially polarized light in coupling to SPPs and in generating sharp plasmonic focal and expands its applicability in applications involving parallel processing.

The SPP field propagating on the metal-air interface was measured by NSOM. We observed strong interference patterns which are the result of coherent interactions between the plasmonic sources propagating towards each other. It should be noted that unlike the typical case where the plasmonic patterns are originated from the structure of the sample (e.g. nanoholes or nanoslits), here the coherent interactions are the result of the structured illumination pattern.

The experimental results are in good agreement with the theory, showing interference fringes having periodicity compatible with the plasmonic SPP wavelength. The measured envelope of the diffraction pattern agrees qualitatively with the simulation results. The measurements show preferred response for light polarized in the direction oriented at 45 degrees with respect to the horizontal axis of the figure. This finding is explained by the polarization response properties of our bended NSOM probe. Finally, the demonstrated approach of generating array of radially polarized plasmonic hot spots on flat metallic film, may be used in myriad applications e.g. microscopy, lithography, sensing and optical memories.

Acknowledgment

This research was funded by the Air Force Office of Scientific Research (AFOSR).

#181718 - $15.00 USD Received 13 Dec 2012; revised 17 Jan 2013; accepted 21 Jan 2013; published 6 Feb 2013